Validation of a new global irrigation scheme in the ORCHIDEE land surface model

Pedro F. Arboleda-Obando[1], Agnès Ducharne[1], Zun Yin[2], Philippe Ciais[3]

[1] Laboratoire METIS UMR 7619, Sorbonne Université, CNRS, EPHE, Paris, 75005, France
[2] Program in Atmospheric and Oceanic Sciences, Princeton University, Princeton, 08540, New Jersey, USA
[3] Laboratoire des Sciences du Climat et de l'Environnement, IPSL, CNRS-CEA-UVSQ, Gif-sur-Yvette, 91191, Essonne, France

Supplement S1

This section shows volumes of water withdrawal for irrigation and of ET increase from ORCHIDEE and AQUASTAT for 1998-2002, as well as the irrigation rate (Sacks et al., 2009) in Fig. S1. Figures S2 and S3 show difference between Irr and NoIrr for additional variables, including energy terms. Figure S4 shows basins included in the analysis of the effect of the new irrigation module, and the corresponding discharge stations. Figure S5 shows the fraction of irrigated paddy rice, with a focus on Southeast Asia. S6 shows the irrigated area for both datasets used on the simulations, HID and LUH2. Finally, S7 shows the spatial distribution of ET bias compared to FLUXCOM, and zonal average values for simulated and observed datasets, and S8 shows the same information (bias modelling compared to LAI3g and zonal average values) for LAI.

We also present two tables. Table S1 shows goodness-of-fit metrics for ORCHIDEE discharge values and observed values from GRDC selected stations. We use four metrics: relative bias (equation 1), the relative change of amplitude of average monthly values (equation 2), the Pearson's correlation coefficient r (equation 3, (Helsel and Hirsch, 1992) and Kling-Gupta Efficiency KGE (equation 4, (Gupta et al., 2009; Kling et al., 2012)).

$$\boldsymbol{B} = \frac{\sum_{i=1}^{n}(\boldsymbol{S_i}-\boldsymbol{O_i})}{\sum_{i=1}^{n}(\boldsymbol{O_i})}.\mathbf{100} \quad (1)$$

$$\boldsymbol{RelAmp} = \frac{\max(S_j)_{j=1,12} - \min(S_j)_{j=1,12}}{\max(O_j)_{j=1,12} - \min(O_j)_{j=1,12}} \cdot \mathbf{100} \quad (2)$$

$$\boldsymbol{r} = \frac{\sum_{i=1}^{n}(S_i - \bar{S}).(O_i - \bar{O})}{\sqrt{\sum_{i=1}^{n}(S_i - \bar{S})^2}.\sqrt{\sum_{i=1}^{n}(O_i - \bar{O})^2}} \quad (3)$$

$$KGE = 1 - \mathrm{ED} = 1 - \sqrt{(r-1)^2 + \left(\frac{\sigma_s}{\sigma_o} - 1\right)^2 + \left(\frac{\mu_s}{\mu_o} - 1\right)^2} \quad (4)$$

Here S and O represents simulated and observed values, respectively, n represents the monthly values from the time-series, j represents one of 12 the months in a year, σ represents the standard deviation, and μ represents the average value, with indices s and o indicating simulated or observed time series.

In table S2 we show the sum of the capacity of dams used for irrigation. We also present the average values at large river basin for irrigated fraction and irrigated paddy fraction, and the bias of evapotranspiration and irrigation. In table S3 we present trends on TWSA from our simulations and from GRACE datasets, the trends of the differences between simulations and GRACE, and the depletion estimates from (Wada et al., 2012).

Text on figures S7 and S8

The NoIrr simulation has a negative bias distribution when we compare this simulation with Fluxcom dataset in irrigated areas (Fig. S7-a). The activation of irrigation in Irr does not correct the distribution of the bias. At the regional scale however, we observe that irrigation activation reduces ET bias, for instance in Southern Asia and India, and in Southern Europe and the Mediterranean (for instance Spain). In China and the US, two irrigation hotspots, the reduction of the negative ET bias in the Irr simulation is small when we compare NoIrr and Irr simulations. Other areas pass from a negative to a positive bias between NoIrr and Irr simulations, for instance in Australia and South America.

The average zonal values at yearly, boreal winter, and boreal summer periods in the irrigated areas (Fig. S7-b) confirm that both simulations NoIrr and Irr underestimate ET when compared to the Fluxcom, with

local exceptions. On the other hand, the activation of irrigation reduces the ET bias for Fluxcom and leads to an overestimation for Gleam. Seasonal effects do not change this general pattern, but the extension and localization of the bias reduction.

In the case of LAI, we observe that the NoIrr simulation has a positive bias when we compare it to the LAI3g dataset (Fig. S8-a) and that this positive bias increases in the Irr simulation, because irrigation enhances transpiration, thus photosynthesis and biomass production. In some areas of India, like the Indus river basin or Middle East, the activation of irrigation reduces a negative bias, but in general, the positive bias increases, for example in China.

The mean zonal values (Fig. S8-b) show that the LAI increase is mostly found in the northern hemisphere and in a small part of the southern hemisphere, roughly following the increase in ET. Seasonally, increases of LAI also are mostly found in the northern hemisphere. For example, in the boreal winter (austral summer, thus high biomass production in the southern hemisphere), just small latitude bands in the southern hemisphere show a statistically detected change due to activation of irrigation. This is probably led by the zonal distribution of irrigated areas, mostly concentrated in the northern hemisphere. Other factors like PFT distribution and local climate could also influence the small effect of irrigation on LAI in the southern hemisphere.

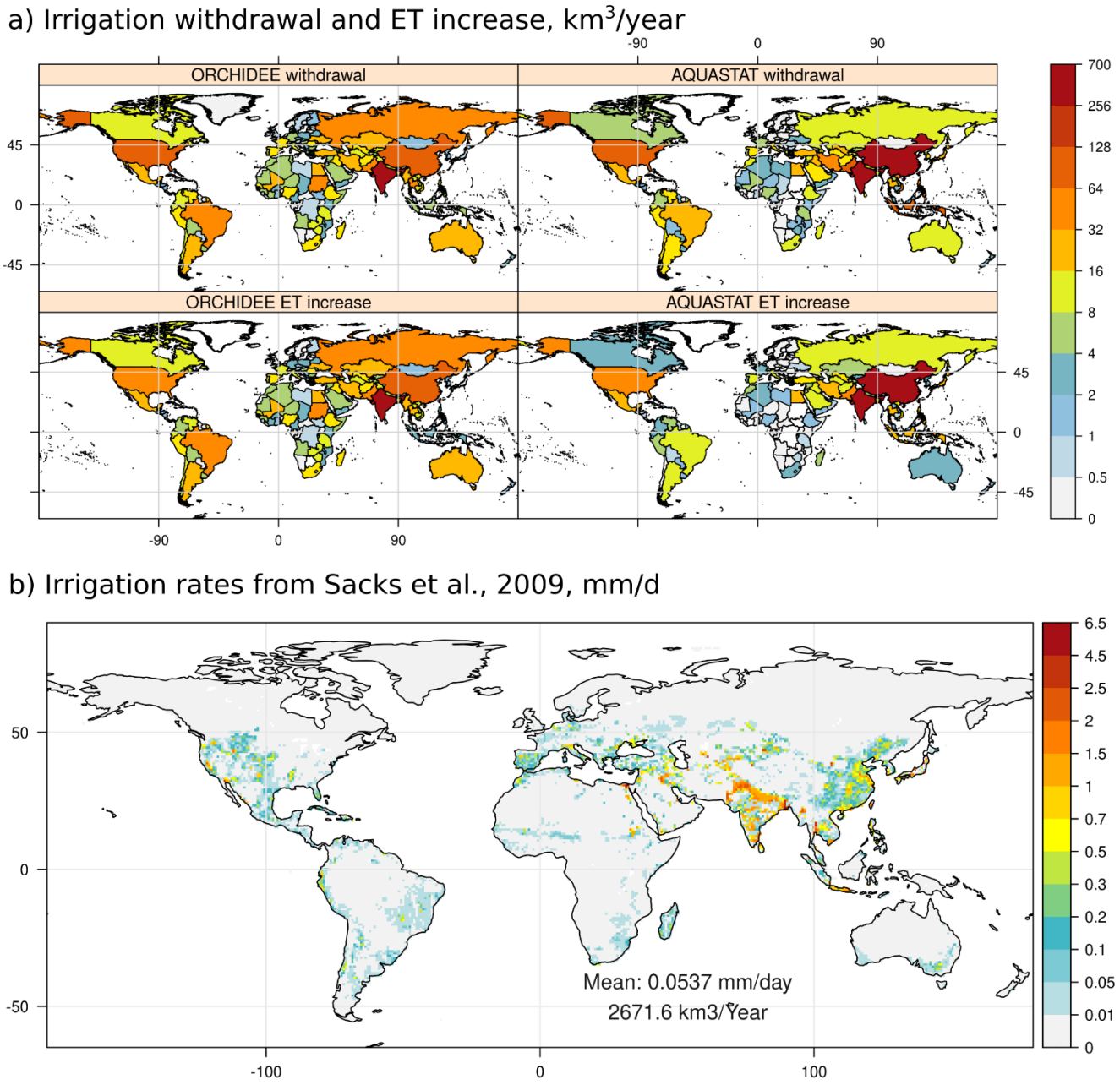

Figure S.1 Volumes of water withdrawal for irrigation and ET increase (called irrigation requirement in AQUASTAT dataset) by country from ORCHIDEE (Irr simulation, average value for 1998-2002), and AQUASTAT (value around 2000), in km^3/year (a). Irrigation rate from (Sacks et al., 2009) for year 2000, mm/d.

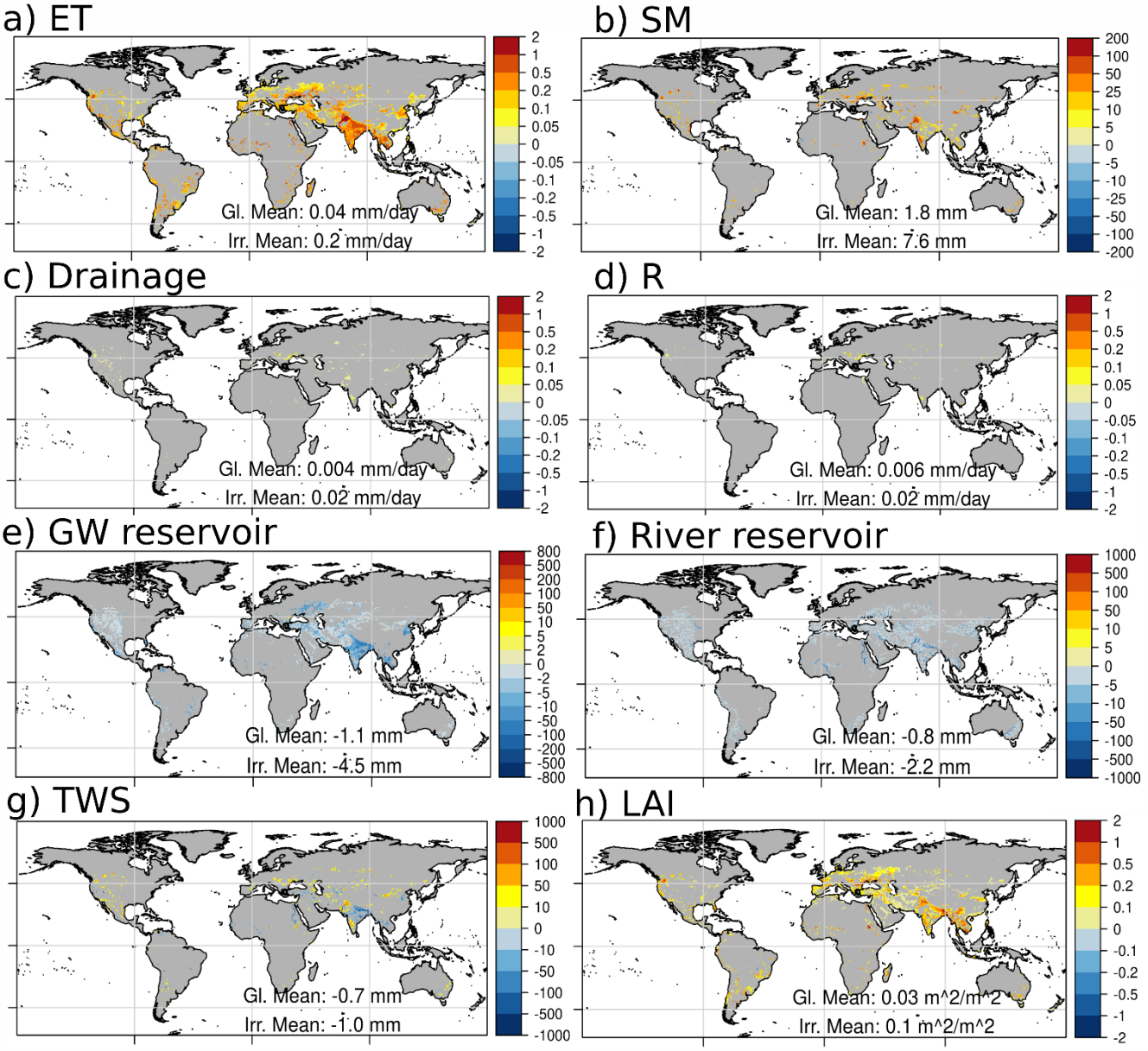

Figure S2 Yearly average difference for 1980 - 2013 between Irr and NoIrr of ET, mm/d (a), SM, mm (b), drainage, mm/d (c), total runoff, mm/d (d), groundwater reservoir, mm (e), river reservoir, mm (f), TWS, mm (g), and LAI, m/m (h). Statistical significance of the mean differences

is tested at each point with a Student's test (p = 0.05). The areas with insignificant changes are left gray.

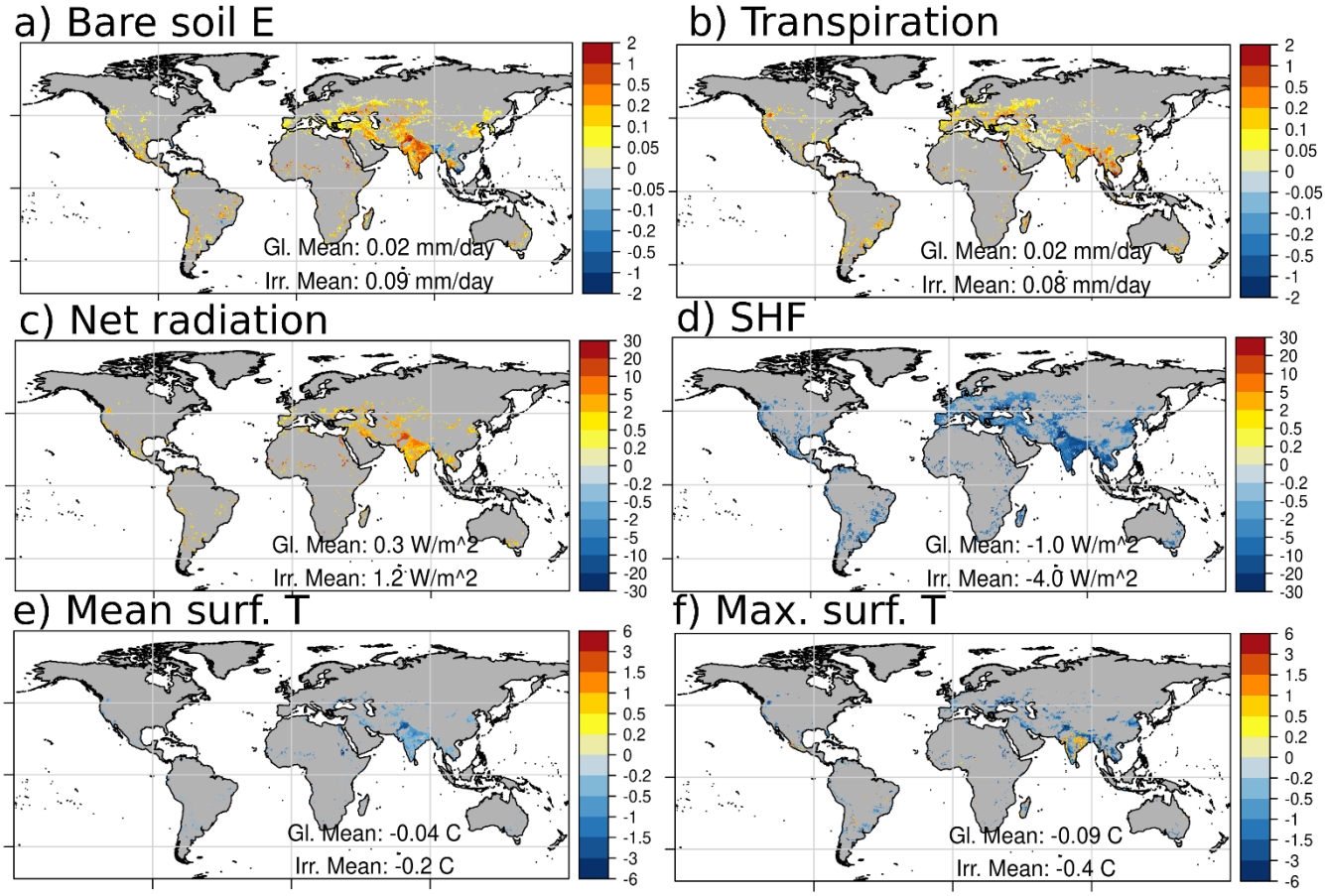

Figure S3 Yearly average difference for 1980 - 2013 between Irr and NoIrr of bare soil E, mm/d (a), T, mm/d (b), net radiation W/m^2 (c), SHF, W/m^2 (d), mean surface temperature, °C (e), and max. surface temperature, °C (f). Statistical significance of the mean differences is tested at each point with a Student's test (p = 0.05). The areas with insignificant changes are left gray.

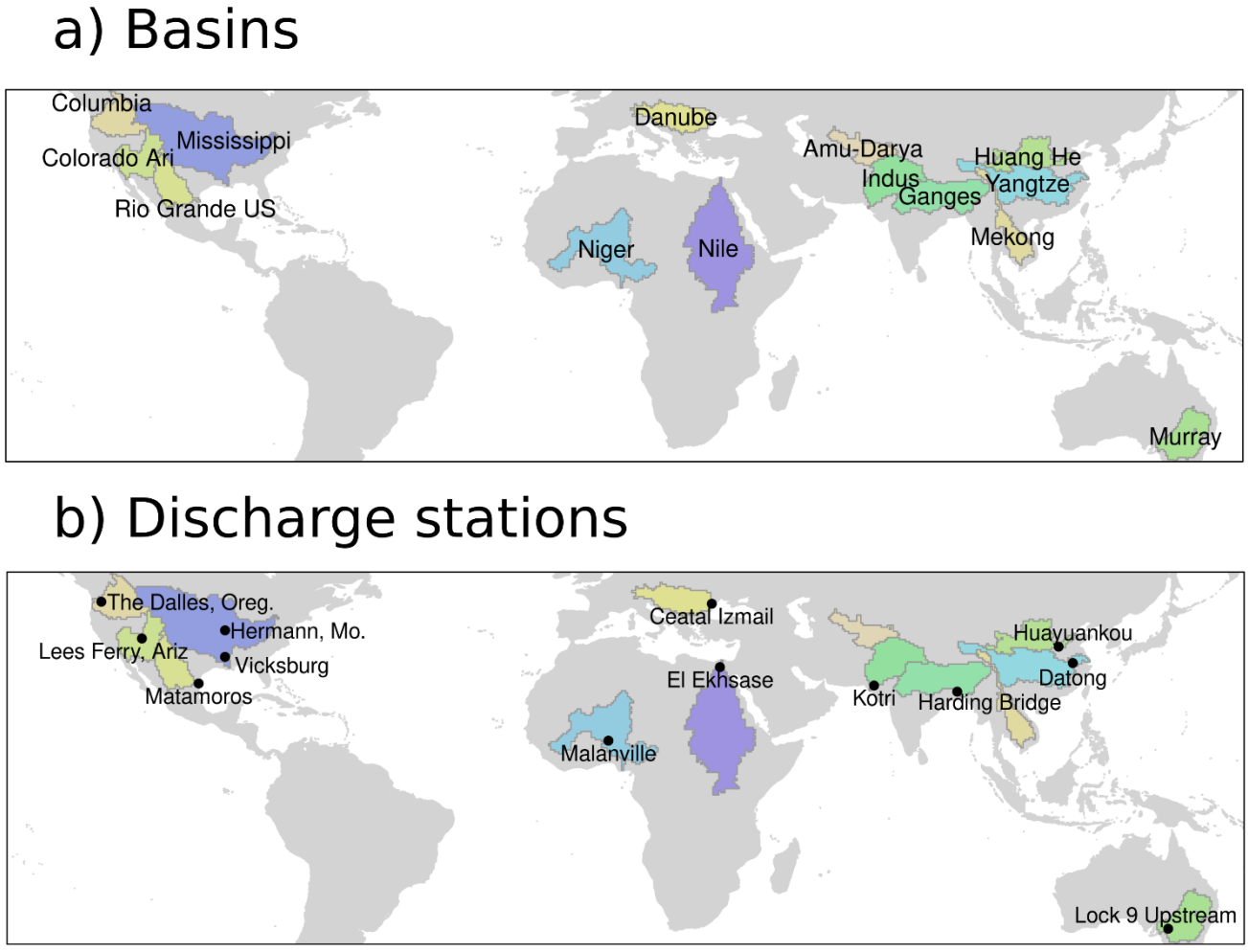

Figure S4 Limits of large basins used in the regional analysis (a). Discharge stations used in the comparison with ORCHIDEE outputs (b).

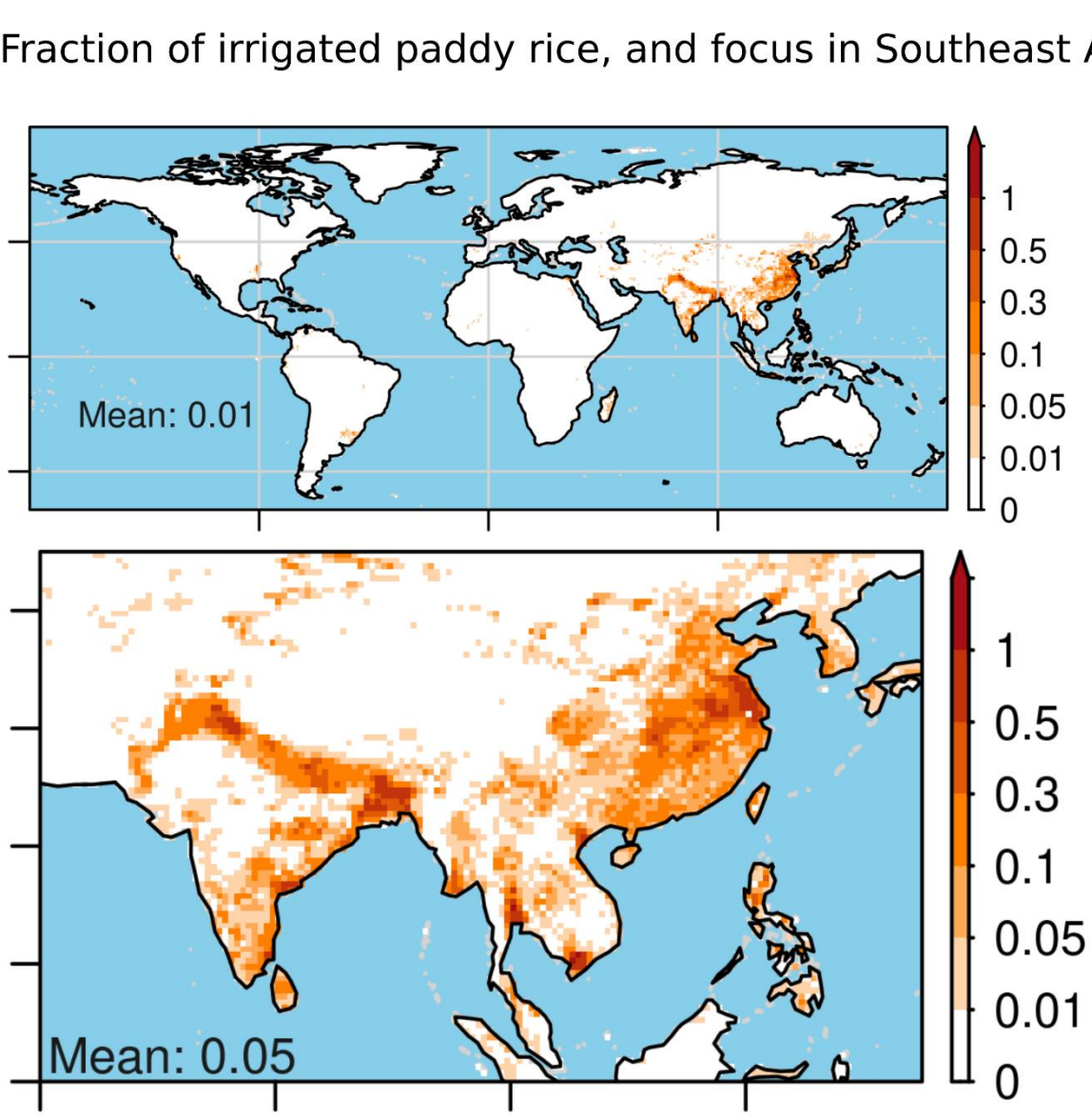

Figure S5 Fraction of irrigated paddy rice, and focus on Southeast Asia. Data comes from MIRCA2000 (Portmann et al., 2010).

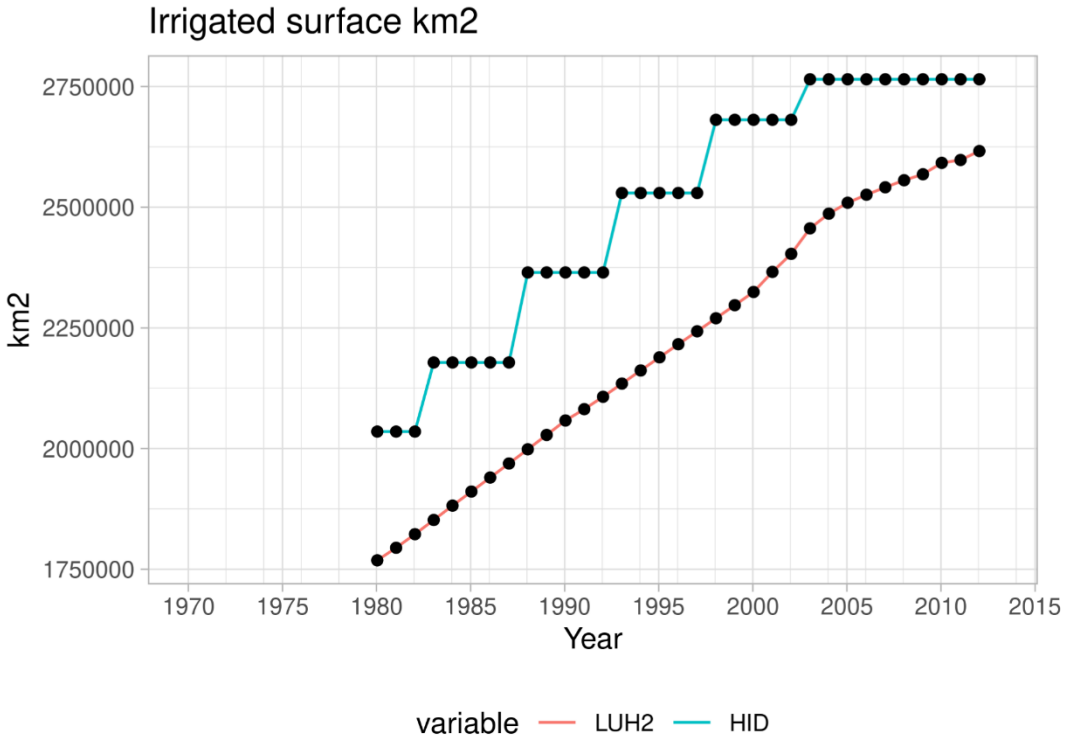

Figure S6 Total irrigated surface in km^2, for HID (Siebert et al., 2015) and LUH2 (Hurtt et al., 2020).

a) ET bias, yearly (mm/d)

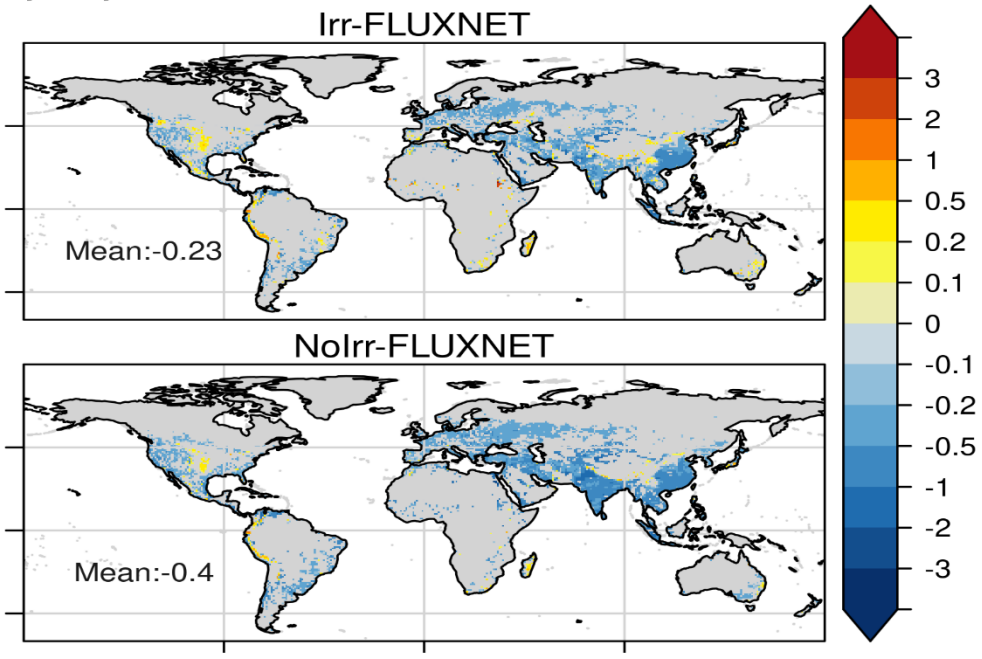

c) ET, zonal average in irrigated areas, mm/d

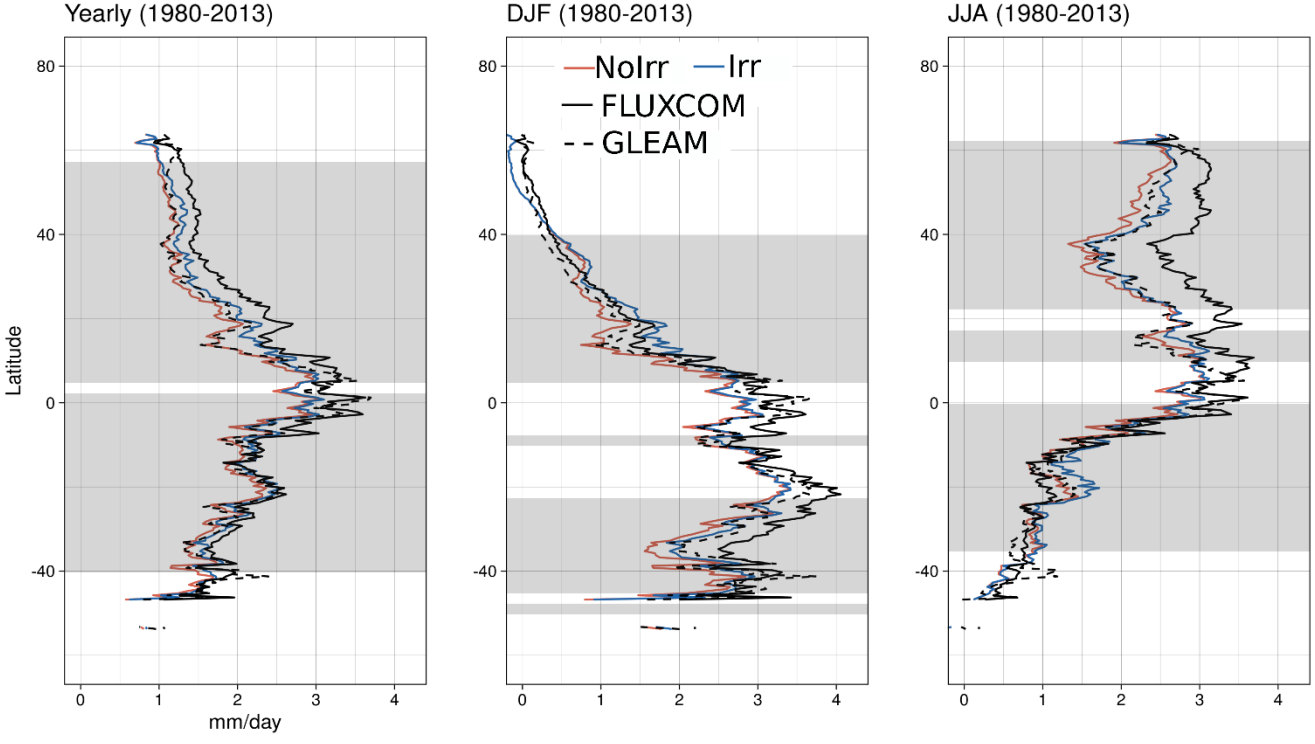

Figure S7 Difference of yearly average values for 1980 - 2013 between NoIrr and Irr simulations, and Fluxcom (a) and for NoIrr and Irr simulations, for ET in mm/d. Statistical significance of the mean differences is tested at each point with a Student's test (p = 0.05). The areas with insignificant changes or no irrigated fraction are left gray. Zonal average values of areas with irrigated fractions for yearly, boreal summer (JJA) and boreal winter (DJF) of ET for period 1980 - 2013 (b) in mm/d. Gray areas for zonal average values depict the latitudes with significant differences between Irr and NoIrr simulation, according to the Student t-test (p = 0.05).

a) LAI bias, yearly (m2/m2)

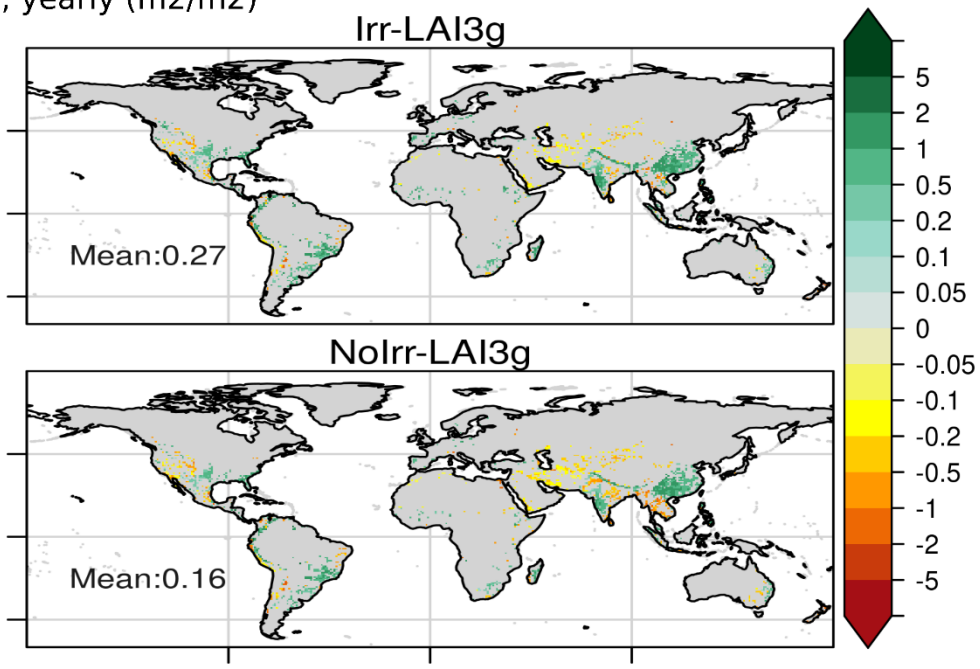

b) LAI, zonal average in irrigated areas, m2/m2

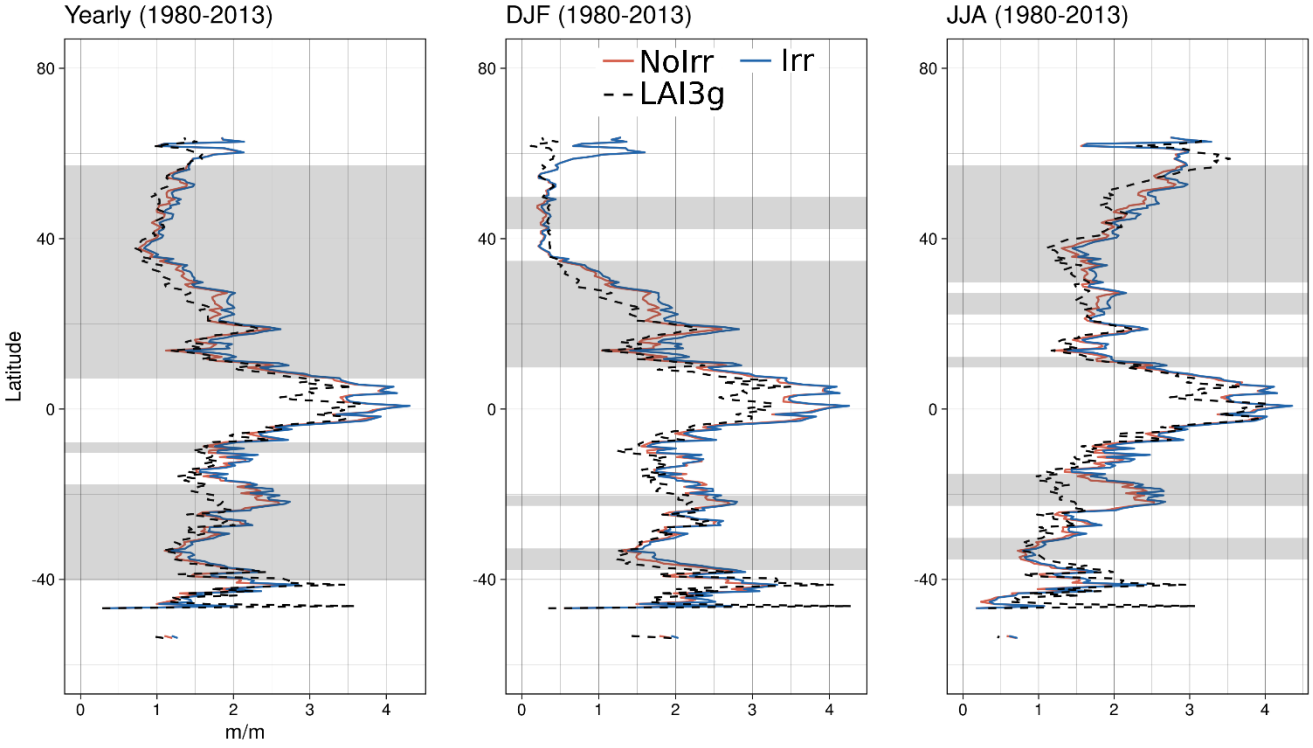

135

Figure S8 Difference of yearly average values for 1980 - 2013 between NoIrr and Irr simulations, and LAI3g (a) for LAI in m^2/m^2. Statistical significance of the mean differences is tested at each point with a Student's test (p = 0.05). The areas with insignificant changes or no irrigated fraction are left gray. Zonal average values of areas with irrigated fractions for yearly, boreal summer (JJA) and boreal winter (DJF) of LAI for period 1980 - 2013 (b) in m^2/m^2. Gray areas for zonal average values depict the latitudes with significant differences between Irr and NoIrr simulation, according to the t-student test (p = 0.05).

Table S1 Goodness-of-fit metrics for ORCHIDEE discharge values and GRDC selected stations. RelAmpli stands for relative change on amplitude, r for Pearson correlation coefficient, KGE for Kling-Gupta efficiency.

	Metric	Irr-NoIrr(%)	Bias %		RelAmpli%		r		KGE	
ID	River@Station		NoIrr	Irr	NoIrr	Irr	NoIrr	Irr	NoIrr	Irr
1	Columbia @ The Dalles, Oreg.	-26.54	-41.43	-56.97	8.47	25.68	0.8	0.69	0.54	0.34
2	Colorado (Ariz.) @ Lees Ferry, Ariz	-42.35	-46.84	-69.36	78.69	134.17	0.08	0.01	-0.03	-0.21
3	Mississippi @ Vicksburg	-5.08	-7.23	-11.94	-54	-47.65	0.62	0.69	0.43	0.49
4	Missouri @ Hermann, Mo.	-24.08	2.24	-22.38	-43.27	-54.33	0.59	0.69	0.59	0.61
5	Rio Grande (MX) @ Matamoros	-81.43	6387.44	1104.72	8349.66	2306.7	0.12	0.13	-71.71	-17.76
6	Nile @ El Ekhsase	-33.43	794.01	495.14	1736.17	1949.26	-0.27	-0.31	-22.15	-23.15
7	Niger @ Malanville	-9.05	506.67	451.77	360.38	373.96	0.58	0.61	-5.25	-4.85
8	Danube @ Ceatal Izmail	-16.76	10.73	-7.83	29.72	23.96	0.67	0.83	0.63	0.66
9	Ganges-Brahmaputra @ Harding Bridge	-25.59	82.23	35.6	7.07	18.49	0.77	0.75	0.15	0.55
10	Yellow River @ Huayuankou	-67.66	-3.93	-68.93	-40.77	-65.64	0.54	0.2	0.39	-0.18
11	Yangtze @ Datong	-2.08	-9.99	-11.87	-36.72	-37.98	0.88	0.88	0.64	0.63
12	Murray @ Lock 9 Upstream	-53.31	832.45	335.41	196.11	84.54	0.47	0.48	-8.13	-3.53
13	Indus @ Kotri	-90.79								
14	Amu-Darya @ Chatly	-65.8								

Table S2 Dams capacity used for irrigation, irrigated fraction and paddy irrigated fraction, ET and irrigation bias at large river basin scale.

Id	Basin	Dams for irrig. $10^6 m^3$	Irrigated fraction	Irrigated paddy fraction	NoIrr-Gleam mm/d	Irr-Gleam mm/d	NoIrr-Fluxcom mm/d	Irr-Fluxcom mm/d	Irrigation bias mm/d
1	Nile	173411	0.010	0.001	0.015	0.114	-0.508	-0.361	0.044
2	Mississippi	16915	0.037	0.002	0.110	0.142	-0.079	-0.047	-0.030
3	Niger	16400	0.001	0.001	0.009	0.055	-0.485	-0.427	0.023
4	Yangtze	19186	0.082	0.091	-0.216	-0.188	-0.370	-0.342	-0.102
5	Ganges	32589	0.178	0.080	-0.016	0.280	-0.364	-0.068	-0.124
6	Indus	44828	0.190	0.052	0.079	0.470	-0.724	-0.323	-0.043
7	Murray	17484	0.021	0.001	-0.006	0.087	-0.162	-0.069	0.067
8	Huang He	2337	0.078	0.021	0.080	0.163	-0.061	0.022	-0.042
9	Colorado Ari	6355	0.021	0.000	0.000	0.053	-0.327	-0.273	-0.031
10	Rio Grande US	19478	0.021	0.000	0.095	0.163	-0.208	-0.140	0.036
11	Danube	1762	0.037	0.000	-0.044	0.080	-0.433	-0.308	0.120
12	Mekong	4379	0.027	0.030	-0.265	-0.068	-0.431	-0.234	0.103
13	Columbia	22713	0.044	0.000	-0.343	-0.245	-0.246	-0.148	-0.038
14	Amu-Darya	25500	0.072	0.002	-0.010	0.161	-0.611	-0.440	-0.073

Table S3 Trends of TWSA values from simulations (NoIrr and Irr) and from the average of GRACE datasets by country, difference between simulated trends and GRACE, and comparison with depletion values from (Wada et al., 2012).

id	Country	NoIrr km^3/y	Irr km^3/y	GRACE km^3/y	NoIrr-GRACE km^3/y	Irr-GRACE km^3/y	Depletion from (Wada et al., 2012) km^3/y
1	India	10.42	8.03	-11.10	27.02	28.46	71.00
2	United States	3.70	3.51	-64.58	69.71	65.08	32.00
3	China	24.57	24.49	-15.16	38.16	38.36	22.00
4	Pakistan	4.78	4.58	1.43	3.28	2.76	37.00
5	Iran	-0.18	-0.28	-20.40	19.93	20.29	27.00
6	Mexico	1.62	1.35	-0.72	3.39	2.93	11.00
7	Saudi Arabia	-1.02	-0.98	-15.71	15.00	15.00	15.00
8	Russian Federation	7.92	7.67	-70.76	69.62	60.27	1.50
9	Italy	0.40	0.42	-0.59	0.86	0.97	2.30
10	Turkey	0.12	0.16	-3.73	3.81	3.61	2.40
11	Uzbekistan	-0.83	-0.79	-2.69	1.81	1.89	4.00
12	Egypt	-0.88	-0.89	-4.49	3.65	3.32	3.00
13	Bulgaria	-0.01	-0.04	-0.63	0.57	0.56	2.00
14	Spain	-0.15	-0.14	0.10	0.33	0.30	1.70
15	Argentina	-11.43	-11.10	-34.76	25.09	25.23	0.90
16	Libya	-1.35	-1.34	-5.70	4.44	4.22	3.10
17	Ukraine	0.71	0.63	-4.69	6.16	5.95	0.30
18	Romania	0.78	0.43	-1.44	1.99	1.82	1.30
19	Kazakhstan	-1.08	-0.79	-18.33	19.06	19.30	2.00
20	South Africa	0.64	0.70	3.92	-3.23	-3.19	1.50
21	Algeria	1.07	1.07	-3.37	4.68	4.90	1.70
22	Greece	-0.17	-0.18	-0.21	0.11	0.10	0.34
23	Morocco	1.09	1.04	1.63	-0.26	-0.19	1.60
24	Australia	17.46	17.78	25.21	-3.25	-4.16	1.00
25	Tajikistan	-0.31	-0.31	-1.08	0.68	0.42	1.20
26	Yemen	-0.11	-0.11	-1.26	1.13	1.15	0.90

27	Turkmenistan	-0.77	-0.70	0.00	-0.86	-0.85	1.25
28	Syria	-0.46	-0.42	-2.32	2.03	2.03	1.23
29	United Arab Emirates	0.10	0.10	-0.19	0.33	0.33	1.18
30	Tunisia	-0.17	-0.16	-0.67	0.54	0.49	0.65
31	Peru	-6.17	-6.20	-4.44	-3.01	-3.74	0.32
32	Bolivia	5.85	5.79	0.61	4.95	5.09	0.25
33	Israel	-0.06	-0.05	-0.13	0.08	0.09	0.38
34	Kyrgyzstan	-0.52	-0.47	-0.78	0.52	0.45	0.31
35	Jordan	-0.12	-0.12	-0.97	0.89	0.85	0.22
36	Mauritania	0.94	0.94	1.12	-0.38	-0.45	0.36
37	Oman	1.08	1.08	-0.69	1.88	1.83	0.20
38	Kuwait	-0.06	-0.06	-0.05	-0.01	0.00	0.25
39	Qatar	-0.01	-0.01	-0.05	0.04	0.04	0.15

References

Gupta, H. V, Kling, H., Yilmaz, K. K., and Martinez, G. F.: Decomposition of the mean squared error and NSE performance criteria : Implications for improving hydrological modelling, J. Hydrol., 377, 80–91, https://doi.org/10.1016/j.jhydrol.2009.08.003, 2009.

Helsel, D. R. and Hirsch, R. M.: Statistical methods in water resources, Stat. methods water Resour., https://doi.org/10.2307/1269385, 1992.

Hurtt, G. C., Chini, L., Sahajpal, R., Frolking, S., Bodirsky, B. L., Calvin, K., Doelman, J. C., Fisk, J., Fujimori, S., Klein Goldewijk, K., Hasegawa, T., Havlik, P., Heinimann, A., Humpenöder, F., Jungclaus, J., Kaplan, J. O., Kennedy, J., Krisztin, T., Lawrence, D., Lawrence, P., Ma, L., Mertz, O., Pongratz, J., Popp, A., Poulter, B., Riahi, K., Shevliakova, E., Stehfest, E., Thornton, P., Tubiello, F. N., van Vuuren, D. P., and Zhang, X.: Harmonization of global land use change and management for the period 850–2100 (LUH2) for CMIP6, Geosci. Model Dev., 13, 5425–5464, https://doi.org/10.5194/gmd-13-5425-2020, 2020.

Kling, H., Fuchs, M., and Paulin, M.: Runoff conditions in the upper Danube basin under an ensemble of climate change scenarios, J. Hydrol., 424–425, 264–277, https://doi.org/10.1016/j.jhydrol.2012.01.011, 2012.

Portmann, F. T., Siebert, S., and Döll, P.: MIRCA2000-Global monthly irrigated and rainfed crop areas around the year 2000: A new high-resolution data set for agricultural and hydrological modeling, Global Biogeochem. Cycles, 24, n/a-n/a, https://doi.org/10.1029/2008GB003435, 2010.

Sacks, W. J., Cook, B. I., Buenning, N., Levis, S., and Helkowski, J. H.: Effects of global irrigation on the near-surface climate, Clim. Dyn., 33, 159–175, https://doi.org/10.1007/s00382-008-0445-z, 2009.

Siebert, S., Kummu, M., Porkka, M., Döll, P., Ramankutty, N., and Scanlon, B. R.: A global data set of the extent of irrigated land from 1900 to 2005, Hydrol. Earth Syst. Sci., 19, 1521–1545, https://doi.org/10.5194/hess-19-1521-2015, 2015.

Wada, Y., Van Beek, L. P. H., and Bierkens, M. F. P.: Nonsustainable groundwater sustaining irrigation: A global assessment, Water Resour. Res., 48, https://doi.org/10.1029/2011WR010562, 2012.